CIRP Annals - Manufacturing Technology 63 (2014) 373–376

Contents lists available at ScienceDirect

CIRP Annals - Manufacturing Technology

journal homepage: http://ees.elsevier.com/cirp/default.asp

Vibration suppression of boring bar by piezoelectric actuators and LR circuit

Atsushi Matsubara (2)[a,*], Minetaka Maeda [b], Iwao Yamaji [a]

[a] Department of Micro Engineering, Kyoto University, Kyoto, Japan
[b] Sinfonia Technology, Mie, Japan

ARTICLE INFO

Keywords:
Chatter
Damping
Piezoelectric actuator

ABSTRACT

This paper presents the vibration suppression of a boring bar using piezoelectric actuators installed in the boring bar, and an inductor-resister (LR) circuit, which acts as a mechanical dynamic absorber. The frequency response function of the compliance was designed so that its real part is constrained to suppress regenerative chatter. The designed boring bar with an optimally tuned LR circuit was set on a lathe to evaluate its dynamic characteristic, and it was found that the chatter vibration was successfully suppressed in the cutting test.

1. Introduction

The vibration between a tool and a workpiece is an important issue in machining operations, as it may deteriorate the workpiece surface quality, lower the productivity, and shorten the tool life. There are various vibration sources in machine tools, tooling systems, and workpieces with supporting jigs. Even though the excitation frequency is located away from the natural frequencies of the structure, regenerative chatter may occur owing to the phase difference between the copied vibration on the surface and the present vibration of the cutting edge. A well-known approach to avoid chatter is based on the analysis of the structure and process dynamics, which provides a stability chart with respect to cutting conditions [1].

Another approach is to improve structure damping with passive or active vibration absorbers. Tuned mass dampers (TMDs) are classical passive vibration absorbers, for which the tuning process was established by Den Hartog [2]. Miguelez et al. investigated several tuning methods for the vibration suppression of a boring bar with a passive absorber [3]. Yang et al. applied multiple TMDs to suppress the structural vibration mode of a CNC lathe and demonstrated the improved performance over a single TMD [4]. Kolluru et al. reported on practical damping devices attached to the workpiece surface to suppress the vibration of thin wall castings [5]. There are also many other passive absorbers such as friction dampers [6] and impact dampers [7]. Passive devices are cost effective and do not need external energy but are inflexible for changing the mechanical parameters.

To extend the efficiency and the flexibility in vibration suppression, active dampers have been investigated. Munoa et al. developed a biaxial inertial actuator and installed it to a ram-type machine tool; they investigated several control laws by using this setup [8]. Ast et al. applied piezoelectric actuators with a frequency-shaped LQG design to suppress the resonance peaks of low-frequency modes [9]. Brecher and Shulz developed an electrohydraulic active damping system that suppresses a dominant structural vibration [10]. Verl and Fley designed an electrohydraulic actuator in a guideway system that controls the damping through friction [11].

The active control systems could provide higher control performance and flexibility in many applications [12]. However, the feedback stability, which is constrained by the responses of the sensors, actuators, and signal processing systems, should be carefully checked. To increase control flexibility in the dynamic absorber design, Yamada et al. proposed a hybrid absorber that uses plate-type piezoelectric actuators together with an electrical inductor-resister (LR) circuit to suppress the vibration of a thin cantilever [13].

In this study, we applied a hybrid absorber with piezoelectric actuators and an LR circuit to suppress the chatter vibration of a boring bar. To provide sufficient force and stiffness, stack-type piezoelectric actuators were devised in a boring bar, and the equal peaks method was used for the optimization of the LR parameters referring the real part of the compliance. A validation test was carried out on a lathe to characterize the performance of the designed absorber.

2. Vibration absorber and dynamic model

Fig. 1 shows a boring bar with a hybrid absorber. The boring bar is the main structure and is modeled as a cantilever. A piezoelectric device is equipped in the bar and shunted with a serial LR circuit. The equivalent mechanical model is shown in Fig. 2. The coupled mechanical and electrical dynamics are described in the following governing equations:

$$M_b\ddot{x} + K_b x + \Theta_b\left(\frac{\Theta_b}{C_p^S}x - \frac{1}{C_p^S}q\right) = f_c \quad (1)$$

* Corresponding author. Tel.: +81 75 383 3675; fax: +81 75 383 3675.
E-mail address: matsubara@prec.kyoto-u.ac.jp (A. Matsubara).

http://dx.doi.org/10.1016/j.cirp.2014.03.132
0007-8506/© 2014 CIRP.

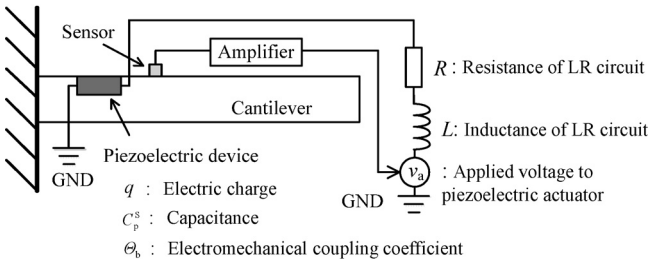

Fig. 1. Schematic of boring bar with hybrid absorber.

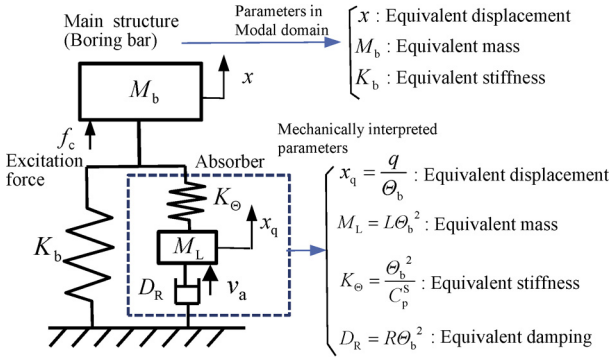

Fig. 2. Equivalent model.

$$L\ddot{q} + R\dot{q} + \frac{1}{C_p^S}q = \frac{\Theta_b}{C_p^S}x + v_a \tag{2}$$

The mechanical representation of Eqs. (1) and (2) are given as follows:

$$M_b\ddot{x} + K_b x + K_\theta(x - x_\theta) = f_c \tag{3}$$

$$M_L\ddot{x}_q + D_R\dot{x}_q + K_\theta(x_q - x) = v_a \tag{4}$$

As shown in Fig. 2, the inductance and resistance of the LR circuit can be interpreted as the absorber mass and damping, respectively, whereas the absorber stiffness is decided by the piezoelectric parameters. Note that the absorber damper is hooked to the ground in this configuration.

A hybrid absorber to increase the control capability is shown in [13]. The acceleration of the main structure is fed back to the command voltage for the piezoelectric actuator.

$$v_a = -\alpha_A \frac{\Theta_b}{C_p^S}\frac{1}{\Omega^2}\ddot{x} \tag{5}$$

where α_A is a gain factor.

3. Optimum tuning

3.1. Equal peaks method

In the classic design of a vibration absorber, the two peaks of the magnitude in the structural compliance are equalized. Yamada [13] applied the two peaks method to determine the LR parameters referring to the magnitude of the compliance. For regenerative chatter repression, however, the real part of the compliance is important. Sims shows the analytical solution for the two peaks method referring to the real part of the compliance [14], in which an absorber is passive and hooked to the main structure. Here, the solution for our case is shown.

Transferring Eqs. (3) and (4) to the frequency domain, nondimensional compliance can be obtained as

$$\frac{X}{X_{st}} = \frac{1}{1 - g^2 + \beta\frac{-(1+\alpha_A f^2)g^2 + 2j\varsigma fg}{f^2 - g^2 + 2j\varsigma fg}} \tag{6}$$

where the following nondimensional terms are used:

$X_{st} = F_c/K_b$: static deflection of the main structure.
$\Omega = \sqrt{K_b/M_b}$: main structure natural frequency.
$\omega_a = \sqrt{K_\theta/M_L} = \sqrt{1/LC_p^S}$: absorber natural frequency.
$g = \omega/\Omega$: nondimensional excitation frequency.
$f = \omega_a/\Omega$: frequency ratio.
$\beta = K_\theta/K_b$: stiffness ratio.
$\zeta = \frac{D_R}{2\sqrt{M_L K_\theta}} = \frac{R}{2}\sqrt{C_p^S L}$: absorber damping ratio.

Note that the frequency ratio and absorber damping ratio can be tuned using LR parameters.

The real part of the compliance in Eq. (6) is calculated as follows:

$$u_R = Re\left[\frac{X}{X_{st}}\right] = \frac{A_h + 4\zeta^2 B_h}{C_h + 4\zeta^2 D_h} \tag{7}$$

$$A_h = (f^2 - g^2)\{(1 - g^2)(f^2 - g^2) - \beta(1 + \alpha_A f^2)g^2\} \tag{8}$$

$$B_h = f^2 g^2(1 + \beta - g^2) \tag{9}$$

$$C_h = \{(1 - g^2)(f^2 - g^2) - \beta(1 + \alpha_A f^2)g^2\}^2 \tag{10}$$

$$D_h = f^2 g^2(1 + \beta - g^2)^2 \tag{11}$$

Fig. 3 plots u_R for different absorber damping ratios ζ_a, where the u_R passes three locked points P_C, Q_L, and Q_R. The frequency ratios for P_C, Q_L, and Q_R can be calculated as

$$g_c = \sqrt{1 + \beta} \tag{12}$$

$$g_{L,R} = \sqrt{\frac{1 + \beta + (1 + \alpha_A\beta)f^2 \mp \sqrt{(1 + \beta + (1 + \alpha_A\beta)f^2)^2 - 4f^2}}{2}} \tag{13}$$

where the suffices "c," "L," and "R" mean locked points in the "center," "left," and "right," respectively.

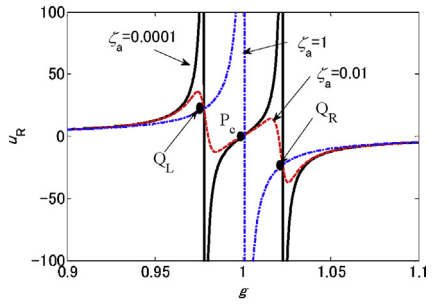

Fig. 3. Calculated u_R for different absorber damping ratios.

The optimal frequency ratio f_{optN} that suppresses the negative peak of u_R can be calculated by setting P_C and Q_R at the same level. Similarly, the optimal frequency ratio f_{optP} that suppresses the positive peak of u_R can be obtained by setting P_C and Q_L at same level. Such optimal frequency ratios are obtained as follows:

$$f_{optP,optN} = \sqrt{\frac{4 + (5 + 2\alpha_A(1 + \beta))\beta \mp \sqrt{\beta^2 + 4\beta(1 + \beta)(2 + \alpha_A\beta)(1 + (1 + \beta)\alpha_A)}}{2(2 + \alpha_A\beta)}} \tag{14}$$

The damping ratios that make u_R have an extreme value at Q_L, P_C, and Q_R are

$$\zeta_L = \frac{1}{2}\sqrt{\left.\frac{B_h C_h' - D_h A_h'}{D_h B_h' - B_h D_h'}\right|_{g=g_L}} \tag{15}$$

$$\zeta_C = \frac{1}{2}\sqrt{\left.\frac{A_h C_h' - C_h A_h'}{C_h B_h' - A_h D_h'}\right|_{g=g_C}} \tag{16}$$

$$\zeta_R = \frac{1}{2}\sqrt{\left.\frac{B_h C_h' - D_h A_h'}{D_h B_h' - B_h D_h'}\right|_{g=g_R}} \tag{17}$$

respectively, where the dash denotes the partial differentiation with respect to g^2. The optimum damping ratios that minimize the positive and negative peaks are set as

$$\zeta_{\mathrm{optP}} = \frac{1}{2}\left(\zeta_L|_{f=f_{\mathrm{optP}}} + \zeta_C|_{f=f_{\mathrm{optP}}}\right) \tag{18}$$

$$\zeta_{\mathrm{optN}} = \frac{1}{2}\left(\zeta_C|_{f=f_{\mathrm{optN}}} + \zeta_R|_{f=f_{\mathrm{optN}}}\right) \tag{19}$$

Finally, the inductance and resistance that give optimum damping are given as follows:

$$L_{\mathrm{optP,optN}} = \frac{1}{f_{\mathrm{optP,optN}}^2}\frac{1}{C_p^S}\frac{1}{\Omega^2} \tag{20}$$

$$R_{\mathrm{optP,optN}} = 2\zeta_{\mathrm{optP,optN}}\frac{1}{f_{\mathrm{optP,optN}}}\frac{1}{C_p^S}\frac{1}{\Omega} \tag{21}$$

Note that the optimum frequency ratio and damping are represented by the stiffness ratio β, whereas they are represented by the mass ratio for the absorber damper hooked to the main structure.

Modification of the optimum parameters is necessary for implementation as follows (see Appendices A and B):

$$L_{\mathrm{optP,optN}} = \frac{1}{(1\mp 2\gamma) f_{\mathrm{optP,optN}}^2}\frac{1}{C_p^S}\frac{1}{\Omega^2} \tag{22}$$

$$R_{\mathrm{optP,optN}} = \frac{2\zeta_{\mathrm{optP,optN}} - \tan\delta}{\sqrt{1\mp 2\gamma}\, f_{\mathrm{optP,optN}}}\frac{1}{C_p^S}\frac{1}{\Omega} \tag{23}$$

where δ is the dielectric loss tangent of the piezoelectric actuator and γ is the damping ratio of the host structure.

3.2. Simulation

The simulation is carried out to check whether the obtained solution can suppress the vibration peaks. Here, dielectric loss of the piezoelectric actuator and the damping of the host structure are neglected. First, the passive case, in which $v_a = 0$, is simulated. Fig. 4 shows the magnitude u_M and the real part u_R of the nondimensional compliance with passive absorbers. For comparison, magnitude optimization [13] is also shown in the figure. As seen in these figures, the positive and negative peaks of the real part are suppressed by using each set of optimum parameters. From the nondimensional compliance, stability charts are calculated for orthogonal cutting. Fig. 5 shows the calculated stability lobes, in which κ in the vertical axis is the multiplication of the cutting coefficient, the width of cut, and $1/K_b$. As seen in Fig. 5, the negative peak optimization increases the upper limit of the unconditional stability zone.

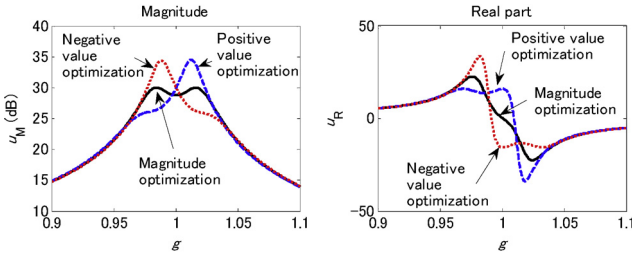

Fig. 4. Comparison of compliance (u_M and u_R) with different optimization schemes ($\beta = 0.002$).

Fig. 6 shows the compliance with the hybrid absorber assisted by the acceleration feedback with various gain factors α_A. The design parameters used are given in the experiment in Section 4. As shown in this figure, vibration suppression can be extended as the gain factor increases.

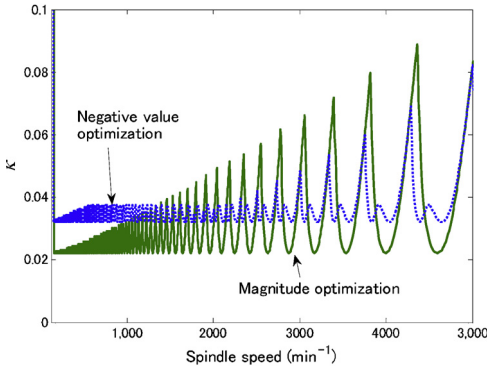

Fig. 5. Comparison of stability limits ($\beta = 0.002$, $\Omega = 1000\pi$).

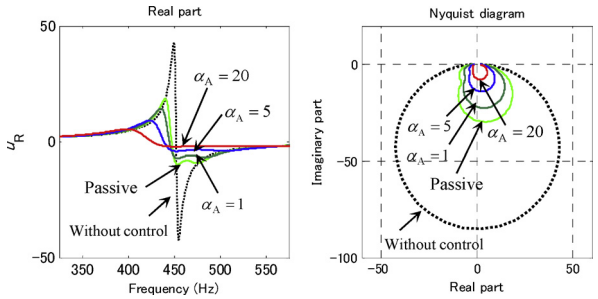

Fig. 6. Compliance with hybrid absorber.

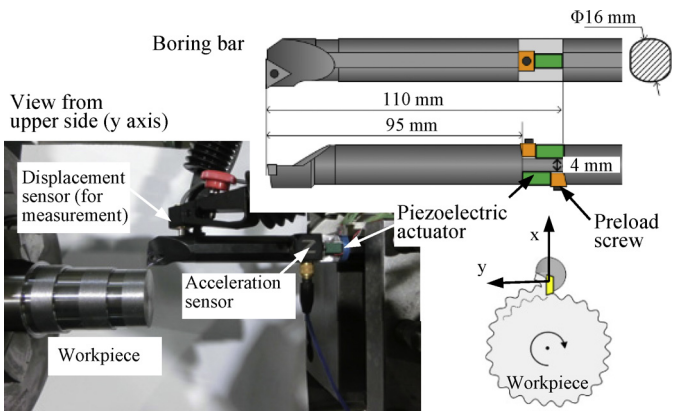

Fig. 7. Boring bar and experimental setup.

4. Experiment

A boring bar was machined, and two piezoelectric actuators were installed with preload. Fig. 7 shows the schematic of the boring bar and the experimental setup. The boring bar was fixed to the tool post of a lathe, and its compliance was measured by an impact hammering test. A machining test was carried out to determine the chatter frequency. For convenience, the test was carried out in the external turning operation. Table 1 lists the fundamental test conditions. In the test, the chatter vibration occurred at 398.3 Hz. The most correlated vibration mode was found in the measured

Table 1
Cutting conditions.

Tool material	TiAlN coated carbide
Tool corner radius	0.2 mm
Tool rake angle	8°
Tool extension	120 mm
Workpiece material	Normal carbon steel (C 0.45%)
Feed rate	0.2 mm/rev
Cutting speed	31.8 m/min
Depth of cut	0.1 mm
Spindle speed	270 min^{-1}
Cutting fluid	None

Table 2
Design parameters.

M_b (kg)	K_b (kN/m)	D_b (Ns/m)	C_p^S (nF)	θ_b (N/V)	β (−)	tan δ (−)
0.0822	574	5.07	657	0.0224	0.00124	0.057

Table 3
Optimized and identified LR parameters.

Optimized in calculation		Identified in experiment	
L_{optP} (H)	R_{optP} (Ω)	L (H)	R (Ω)
0.237	52.0	0.256	56.5

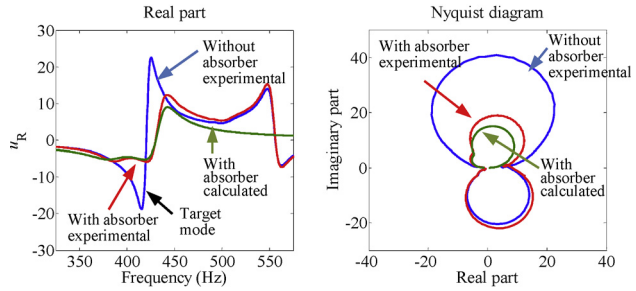

Fig. 8. Compliance G_{xy} with and without the hybrid absorber ($\alpha A = 10$).

compliance from the force in the y direction to the displacement in the x direction (referred to as G_{xy}), which was set as the target mode. The equivalent mechanical parameters were identified and are presented in Table 2 together with the piezoelectric parameters. Using the LR parameters calculated from Eqs. (22) and (23), an electric circuit was fabricated. The optimized parameters are listed in Table 3 together with those identified in the experiment.

After the implementation of the absorber, the compliance was measured, and a cutting test was carried out again. Fig. 8 shows the measured compliance G_{xy} with and without the hybrid absorber, in which acceleration feedback was employed with a gain factor of $\alpha_A = 10$. The calculated compliance in which the boring bar was modeled with the target mode is also shown in the figure. Note that positive-peak-tuning parameters are used owing to the negative sign of the cross transfer function. As can be seen in this figure, the negative peak is as successfully suppressed as the calculated one. Fig. 9 shows the measured displacements during the cutting test. The vibrations were decreased by 17 dB and 20 dB in the x and y directions, respectively, which proves that the designed hybrid absorber can reduce the chatter vibration.

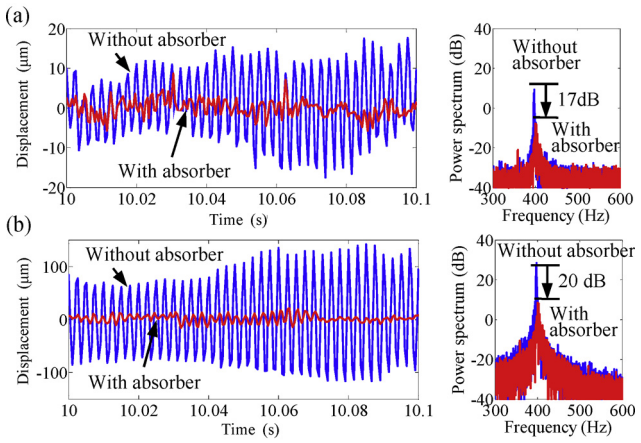

Fig. 9. Measured displacements in the machining: (a) x-direction and (b) y-direction.

5. Conclusions

A hybrid absorber with piezoelectric actuators and an LR circuit was designed to suppress the vibration of a boring bar. The optimized LR parameters were derived analytically, holding the real part peaks of the compliance. The performances of the passive and hybrid absorbers were compared in the simulation. With the parameter modification for the dielectric loss and host structure damping, an LR circuit was implemented in the experimental device. The test results validate the design and its performance.

Appendix A

Dielectric loss of the piezoelectric elements will affect the tuning, which can be modeled using a serial resistance [13]:

$$R_\delta = \frac{\tan\delta}{\omega C_p^S}$$

where δ is dielectric loss tangent. The damping ratio of this resistance is estimated as

$$\zeta_\delta = \frac{f\tan\delta}{2g} \approx \frac{\tan\delta}{2}$$

Note that $f = g = f_{optP,optN}$ is used for the approximation.

Appendix B

In the case in which the host structure has a damping D_b and its damping ratio is γ, the frequency ratios that give the extreme values to the real part of the compliance of the host structure alone are $\sqrt{1 \mp 2\gamma}$. These sifts should be considered in the "real part" optimization. Here we simply modify the optimum frequency ratios as follows:

$$f'_{optP,optN} = \sqrt{1 \mp 2\gamma}\, f_{optP,optN}$$

References

[1] Altintas Y, Weck M (2004) Chatter stability of metal cutting and grinding. *CIRP Ann* 53/2:619–642.
[2] Den Hartog JP (1956) *Mechanical Vibrations*, McGraw-Hill, New York.
[3] Miguelez MH, Rubio L, Loya JA, Fernandez-Saez J (2010) Improvement of chatter stability in boring operations with passive vibration absorbers. *Int J Mech Sci* 52:1376–1384.
[4] Yang Y, Munoa J, Altintas Y (2010) Optimization of multiple tuned mass dampers to suppress machine tool chatter. *Int J Mach Tools Manuf* 50(9):834–852.
[5] Kolluru K, Axinte D, Becker A (2013) A solution for minimising vibrations in milling of thin walled casings by applying dampers to workpiece surface. *CIRP* 62/1:415–418.
[6] Edhi E, Hoshi T (2001) Stabilization of high frequency chatter vibration in fine boring by friction damper. *Precision Eng* 25:224–234.
[7] Ema S, Marui E (2000) Suppression of chatter vibration of boring tools using impact dampers. *Int J Mach Tools Manuf* 40:1141–1156.
[8] Munoa J, Mancisidor I, Loix N, Uriarte LG, Barcena R, Zatarain M (2013) Chatter suppression in ram type travelling column milling machines using a biaxial inertial actuator. *CIRP Ann* 62(1):407–410.
[9] Ast A, Braun S, Eberhard P, Heisel U (2007) Adaptronic vibration damping for machine tools. *CIRP Ann* 56(1):379–382.
[10] Brecher C, Schulz A (2005) Electrohydraulic active damping system. *CIRP Ann* 54(1):389–392.
[11] Verl A, Frey S (2012) Improvement of feed drive dynamics by means of semi-active damping. *CIRP Ann* 61(1):351–354.
[12] Neugebauer R, Denkena B, Wegener K (2007) Mechatronic systems for machine tools. *CIRP Ann* 56(2):657–686.
[13] Yamada K, Matsuhisa H, Utsuno H (2014) Enhancement of efficiency of vibration suppression using piezoelectric elements and LR circuit by amplification of electrical resonance. *J Sound Vibrat* 333:1281–1301.
[14] Sims ND (2007) Vibration absorbers for chatter suppression: a new analytical tuning methodology. *J Sound Vibrat* 301:592–607.